ELSEVIER

A micro pitch and roll motion sensor

Jongbaeg Kim*, Liwei Lin

Department of Mechanical Engineering, University of California at Berkeley, 1113 Etcheverry Hall, Berkeley, CA 94720, USA

Abstract

Characterization of pitch and roll motions of the slider in the hard disk gimbal system is important to achieve higher aerial recording densities. This paper describes a novel piezoresistive-type microsensor that could be directly mounted on the existing slider/gimbal system of a hard disk drive to simultaneously measure the pitch and roll angles of the slider. The size of the fabricated microsensor is designed as 1 mm × 1 mm × 0.1 mm for picoslider applications and the sensor is fabricated by a silicon micromachining process for mass production. The dynamic behavior of the system is slightly altered as expected in a simulation after the sensor is mounted on the slider and the fundamental frequency shift of pitch and roll motion is calculated to be less than 5% of the original system but it is believed that this sensor could provide the best in situ measurement than other currently existing methods. Experimentally, the prototype sensor is capable of detecting pitch and roll angles within ± 3° and the performance is compared with interferometric measurement data and the mismatch is nominally within 14% in average.
© 2003 Elsevier B.V. All rights reserved.

1. Introduction

Dynamic characteristics of the slider have been important parameters for the hard disk design and performance. Numerous researches have been performed on mathematical modeling, simulations, and experiments since the 1970s [1–5]. Typically, a critical parameter in hard disk design is the flying height or spacing between the read/write head and the magnetic medium. Higher aerial recording densities in small size magnetic disk drives are commonly related to the flying height control. Because the slider flies over the surface of the disk with such a small gap, the flying height can be changed by disturbances such as asperities on the disk. In addition to the flying height of the slider, pitch and roll motions shown in Fig. 1 also decide the flying characteristics of the slider. Undesirably large angle of pitch and roll loosen the required small flying height and decreases the reliability of disk drives. Therefore, measuring the pitch and roll angle of the slider is very important for the performance and reliability of magnetic disk drives.

Two different ways have been developed to measure the pitch and roll angles of the slider; capacitive, and optical techniques shown in Fig. 2. The first technique measures the

capacitance between a conducting disk and a slider that is made of conductive ceramic to allow the slider-disk capacitance to be measured [6–8]. Here the slider was constructed in such a manner that each corner was insulated from the rest of the body, to allow determinations of the pitch and roll motions. Each corner of the slider was then electrically connected to a channel of a capacitance bridge. The second method uses optics to measure and compare the length of optical paths, i.e. the phase difference between the two beams using interferometry [9,10]. It requires a transparent disk made of glass or quartz in place of the magnetic disk and two optical beams on two different points on the slider surface to measure the slider's pitch and roll motions.

The capacitive method requires specially fabricated conductive disk and slider, and the electrostatic force caused by the capacitive elements on the slider and disk will change the flying-start characteristics when the disk is accelerated from zero velocity (the flying-start velocity of the disk will increase compared to the real hard disk system). The optical technique, unfortunately, requires a transparent disk which is made of totally different material with that of magnetic disk. Furthermore, in order to measure the pitch and roll angles of the slider, multiple light sources, and detectors are needed, which makes this method complicated and expensive. Currently, the two methods used to measure the slider's dynamic characteristics cannot be used for the real magnetic

* Corresponding author. Tel.: +1-510-642-8983; fax: +1-510-643-6637.
E-mail address: jbkim@me.berkeley.edu (J. Kim).

Nomenclature

a, a', b, b'	distance from the origin of the coordinates to each side of the center plate
A, B, C, D, E, F	specific position on the center plate
E	Young's modulus
I	area moment of inertia
L	length of supporting column
k_i	stiffness of one beam
k_θ, k_β	equivalent torsional stiffness of the gimbal in pitch and roll direction
k'_θ, k'_β	equivalent torsional stiffness of the sensor in pitch and roll direction
k_ϕ	stiffness of supporting column
$\boldsymbol{P}, \boldsymbol{Q}, \boldsymbol{R}$	rotation matrix
$\boldsymbol{T}$	transformation matrix between beam deflections and pitch, roll angles
(x_i, y_i, z_i)	original coordinates of each corner of the center plate of sensor ($i = 1 \sim 4$ denote each of four corner)
(x'_i, y'_i, z'_i)	new coordinate system fixed on the slider surface after pitch motion
(x''_i, y''_i, z''_i)	new coordinate system fixed on the slider surface after pitch and roll motion
(x^*_i, y^*_i, z^*_i)	new coordinate system fixed on the slider surface after pitch, roll and vertical motion
z_c	vertical coordinate of the center of center plate
Δz_i	vertical deflection of ith beam

Greek letters

β	roll angle
ϕ	deflection angle of supporting column
ν	Poisson's ratio
θ	pitch angle
ρ	resistivity of the piezoresistor

disk and Al_2O_3TiC picoslider although optical method has been most widely used in the industry only for the calibration purpose. Because the measured system is not a real hard disk, the tribological characteristics may be different with that of the real disk drives, which diminishes the usefulness of the measured values. Another effort to measure disk-slider interfacial dynamics [11] was to fabricate a silicon gimbal system with integrated piezoresistive sensors on it. However, this approach also alters the whole gimbal system and cannot be used for commercialized hard disk systems.

A different type of sensor which can be applied to a real magnetic disk and slider system is required to preserve the tribological and dynamic characteristics of the measured system and to acquire more accurate slider dynamics. For this, a new type of MEM sensor is designed that could be directly mounted on the slider to minimize the alteration of the measured system and to maintain the tribological and dynamic characteristics.

2. Measurement mechanism

The new sensor designed here is basically a piezoresistive sensor that can dynamically measure the pitch and roll angles concurrently. The sensor is mainly composed of two rigid structures and mechanical springs; a center plate and an outer substrate that are connected together by the four spring elements at each corner. The geometry of the sensor is shown in Fig. 3 along with the location to be mounted in a slider/gimbal system. The center plate is to be attached to the dimple of the suspension arm and the outer substrate is to be attached on the top surface of the slider. When the slider (hence the outer substrate) rotate with respect to the dimple (hence the center plate), each beam will deflect by different amount and pitch and roll angles are the functions of deflected amount of each beam. Beam deflection is measured by the piezoresistors on top of each beam. The sensing mechanism is explained in Fig. 4. Whenever slider has relative motion such as pitch and roll with respect to dimple, each of four beams will deflect by different amount. These small deflections are linearly proportional to the output of piezoresistor, which is in the form of voltage change of the bridge circuit depending on the resistance change. Once the beam deflection is calibrated to the resistance change, pitch
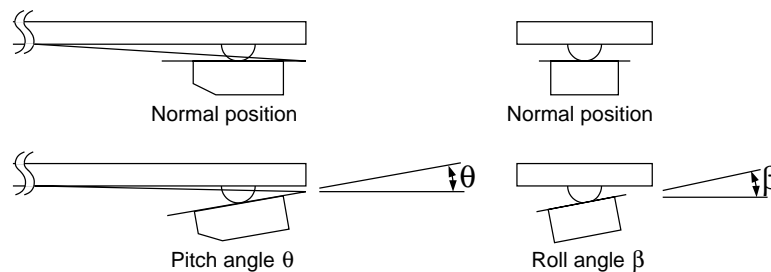

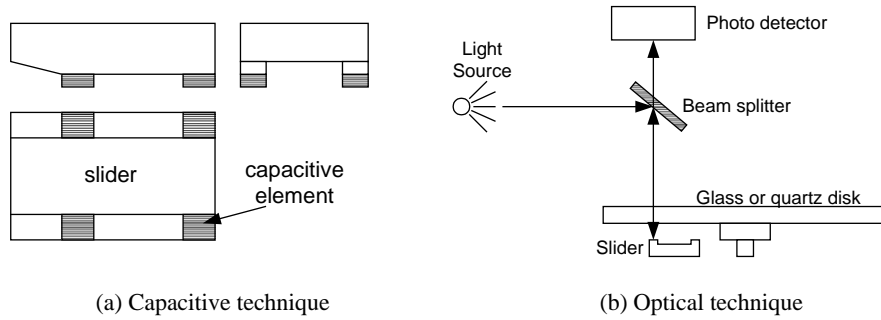Fig. 1. Pitch and roll angle of the slider motion.

(a) Capacitive technique   (b) Optical technique

Fig. 2. Optical and capacitive technique to measure pitch and roll.

Fig. 3. Location for the sensor to be mounted and geometry.
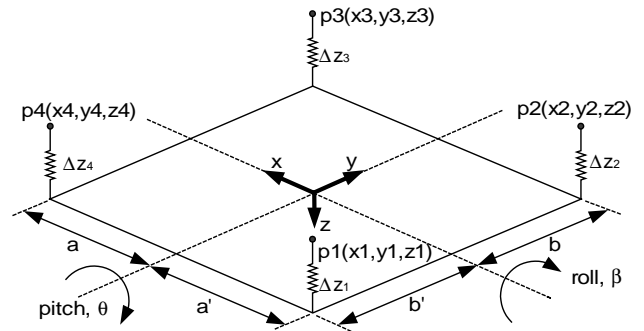

Fig. 5. Cartesian coordinates on the center plate of the sensor.

grees of freedom; pitch, roll, and vertical displacement. This 3-DOF model has been used in numerous dynamic modeling and simulation studies of slider [12–15]. To detect pitch and roll motion from the each measured beam deflection values, appropriate transformation relationship between the two vectors, $\{\Delta z_1, \Delta z_2, \Delta z_3, \Delta z_4\}^T$ which provides beam deflection information and $\{\theta, \beta, z_c\}^T$ which is composed of pitch, roll and vertical displacement of the center of center plate as shown in Fig. 5, should be defined. Because the slider is simplified to have only 3-DOF, three generalized coordinates are necessary and sufficient to describe the slider motion. Therefore, one of Δz_1, Δz_2, Δz_3, and Δz_4 is redundant and any three of them are necessary and sufficient to give all the information about the slider motion. However, the fourth beam balances mechanical stiffness of the sen-

and roll angles are deduced from the piezoresistor outputs through the transformation matrix that relates the linear deflection of beams and angular motion of the slider.

Pitch and roll stiffness values of the gimbal are relatively small compared to the stiffness in lateral (x, y) directions and yaw stiffness. Therefore, it is assumed that a slider has 3 de-
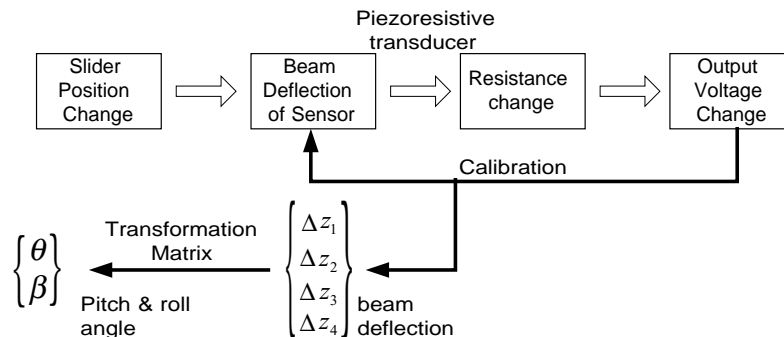

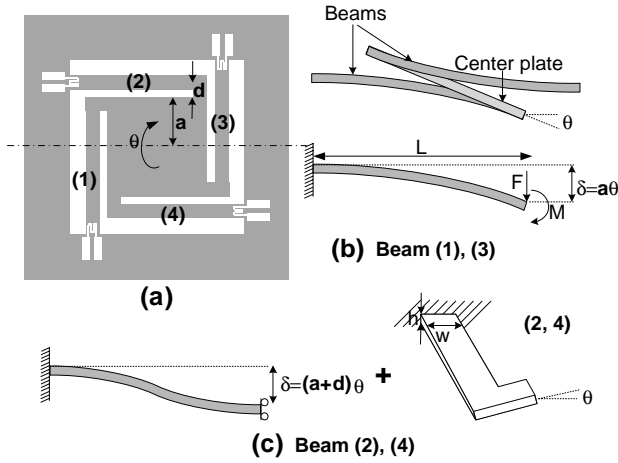Fig. 4. Conceptual diagram of the sensor operation.

Fig. 6. Beam deflections and corresponding boundary conditions for a pitch directional angular displacement of the center plate ((a), configuration of beams and numbering; (b), boundary conditions for beam (1) and (3); (c), boundary conditions for beam (2) and (4).

sor in pitch and roll direction and can be used to verify the deduced angles.

The transformation matrix can be derived by using the rotation matrix of Cartesian coordinates. Suppose the vertical deflection of each of four beams due to the different configuration of the center plate after pitch angle, θ; roll angle, β; and vertical translation, z_c are Δz_i where $i = 1 \sim 4$ denote each of four corner. Assuming small motion, the kinematic relation is derived as

$$\begin{Bmatrix} \Delta z_1 \\ \Delta z_2 \\ \Delta z_3 \\ \Delta z_4 \end{Bmatrix} = \begin{bmatrix} a' & -b' & 1 \\ a' & b & 1 \\ -a & b & 1 \\ -a & -b' & 1 \end{bmatrix} \begin{Bmatrix} \theta \\ \beta \\ z_c \end{Bmatrix} \Rightarrow z_i = T z_c \qquad (1)$$

So the pitch and roll can be related to the beam deflection Δz_i by linear transformation matrix T. The detail of derivation is provided in Appendix A.

3. Sensor structural design

To minimize the alteration of the slider/gimbal structure by the added sensor, the sensor stiffness in pitch and roll direction should be much smaller than that of gimbal. To estimate the equivalent torsional stiffness of the sensor, the boundary conditions and structure geometry must be considered first. For example, when the center plate is rotated in pitch direction for the amount of θ as shown in Fig. 6(a), the deformed shape of beam 1 (and 3) is different from that of beam 2 (and 4). Assuming the center of the square center plate of the sensor is bonded to the dimple of the suspension arm, it is observed that $a' = a = b' = b$. Beam 1 and 3 have the same configuration due to symmetry and their boundary conditions are shown in Fig. 6(b). The total deflection of beam 1 (and 3) is the combination of linear deflection and bending moment from the rotation of the

center plate. For beam 2 (and 4), both bending and torsion occur at the same time. However, under the current configuration, the piezoresistors are not sensitive to this torsion due to their orientation such that the kinematic relation derived in Eq. (1) is still valid. The boundary condition in this case is shown in Fig. 6(c) and the combination of both bending of fixed-guided beam and torsion of rectangular beam will be the stiffness of beam 2 (and 4). When the stiffness of beam 1 and 3 after the boundary conditions are considered is k_1, their contribution to the pitch and roll stiffness of the sensor is $k_{\theta 1} = k_{\theta 3} = a^2 k_1$. Likewise, when the stiffness of beam 2 and 4 is k_2, their contribution is $k_{\theta 2} = k_{\theta 4} = (a + d)^2 k_2$. Then the total pitch and roll stiffness k'_θ and k'_β due to the beams of the sensor is the summation of $k_{\theta 1} \sim k_{\theta 4}$. After the sensor is attached on the slider, the total gimbal stiffness will be $k_\theta + k'_\theta$ for pitch and $k_\beta + k'_\beta$ for roll motion, where k_θ and k_β are the gimbal stiffness without the sensor. One of the design criteria put here is that the additional stiffness is not more than 10% of the original gimbal stiffness. The geometry and the thickness of four beams are decided by this criterion.

The current geometry of the sensor shows very small values of stiffness with respect to pitch and roll. Not only that, the vertical directional stiffness, k_z is also very small. The commercial slider–gimbal–suspension systems are assembled with a pre-load of 2–3 g (20–30 mN) [16] between a slider and a pivot of a suspension arm, which is too large for the microsensor to sustain. Therefore, the sensor structure requires additional structure that can sustain the pre-load while it does not increase the stiffness in pitch and roll direction significantly. To achieve this goal, a vertical column structure underneath the center plate is designed as shown in Fig. 7. This column works like a cantilever beam with the center plate at the end deformed by a moment applied on that end to allow pitch and roll motion. The dimension of the supporting column also can be decided from the stiffness criterion. Suppose the maximum stiffness of the supporting column cannot be more than 10% of the equivalent gimbal stiffness for pitch and roll to reduce the effect of this column on the whole system stiffness. Then from the fixed-hinged beam relation, the torsional stiffness contribution of supporting column is

$$M = \frac{4EI}{L}\phi, \qquad k_\phi = \frac{4EI}{L} \le 0.1 k_\theta. \qquad (2)$$
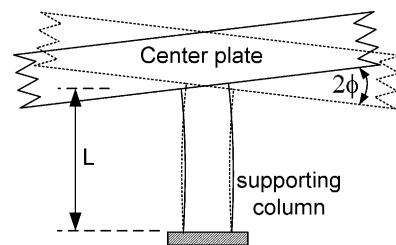

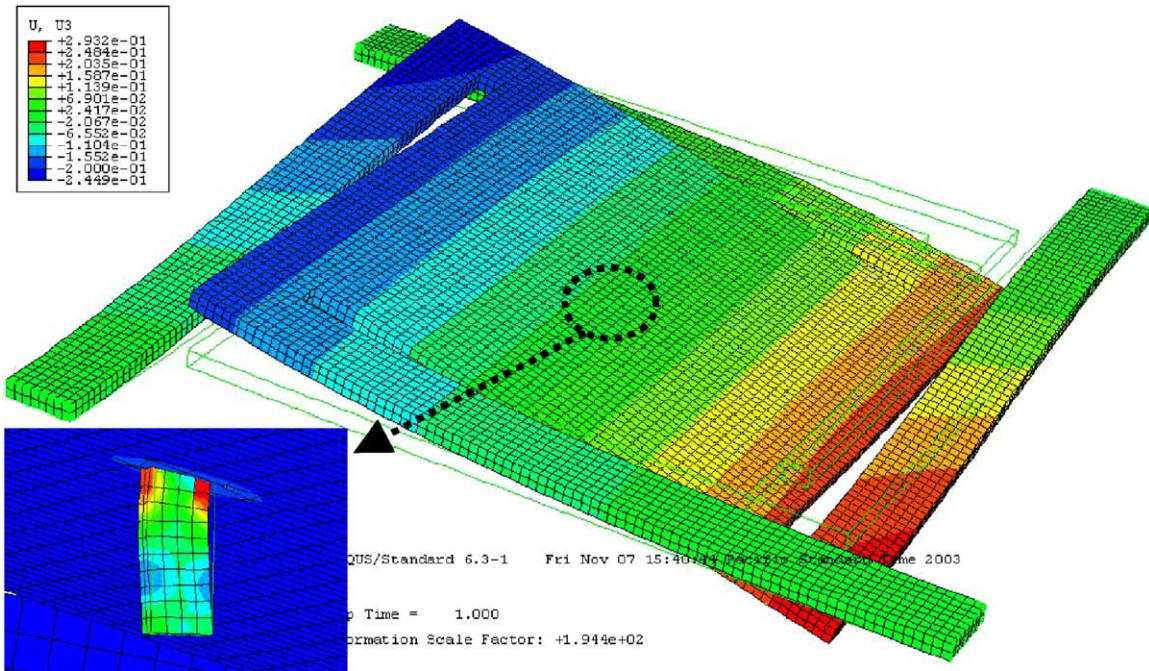Fig. 7. Motion of the vertical column underneath the center of the center plate.

Fig. 8. Finite element analysis to estimate equivalent torsional stiffness of sensor structures (plotted result is the displacement solution for a pitch directional angular displacement of center plate).

For a rectangular cross-sectional supporting column with a side length of ∼6 μm satisfies this criteria when L is 20 μm. A finite element model was built to assist the final dimensions of the center plate, beams and supporting column. Fig. 8 shows the deflection simulation result after anisotropic etching. It is noted that in the FE model, the column is approximated as a 9 μm × 6 μm rectangular cross-section but the real shape of supporting column is hexagonal. The final dimension of the sensor is presented in Fig. 9 based on the FEA simulations, where the thickness of beams and center plate is 12 μm. It is found that analytical model gives higher sensor stiffness than the FE model because the short portion of the L-shape beam and the center plate were assumed to

be rigid in the analytical model. Table 1 lists typical inertia and stiffness parameters of picoslider and gimbal along with the additional inertia and stiffness of the sensor obtained from the finite element analysis. The slight mismatch between pitch and roll stiffness comes from the non-square cross-section of the supporting column.

Fig. 10 shows the altered slider/gimbal system after the sensor is mounted. The beams and supporting column of the sensor now work as springs added to the original gimbal stiffness in parallel. The total stiffness of the gimbal in pitch and roll direction has increased by 20% based on the current design geometry as compared to the original system without the sensor mounted. The sensor also adds inertia to the slider in both pitch and roll direction. The combined effect of additional stiffness and inertia is predicted in Fig. 11 by using MATLAB simulation. The damping coefficient $\zeta = 0.002$ for pitch and roll motion of slider for this calculation was adopted from reference [5]. For a typical unloaded picoslider and gimbal system, it is observed that
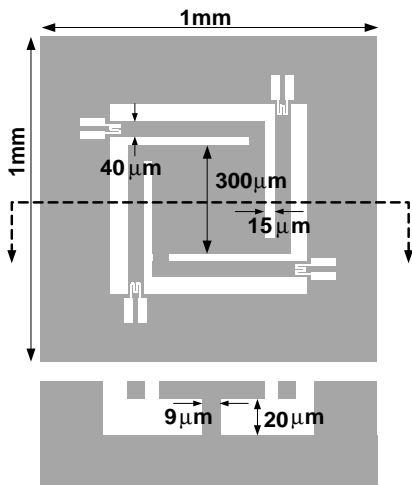

Fig. 9. Dimension of the sensor that meets stiffness requirement.

Table 1
Dynamic properties of slider/gimbal (from [5]) and the sensor

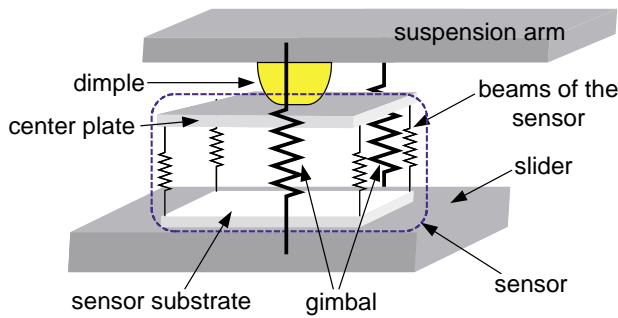|	Slider/gimbal	Sensor
Dimension	1.25 mm × 1 mm × 0.3 mm	1 mm × 1 mm × 0.1 mm
Mass	1.59 mg	0.233 mg
Mass moment of inertia (in pitch direction)	2.19 × 10⁻¹³ kg m²	2.02 × 10⁻¹⁴ kg m²
Pitch stiffness	$k_\theta = 46{\sim}74$ μNm/rad	$k'_\theta = 14$ μNm/rad
Roll stiffness	$k_\beta = 34{\sim}63$ μNm/rad	$k'_\beta = 11 \sim 14$ μNm/rad

Fig. 10. Altered slider/gimbal system after the sensor is mounted.

the fundamental frequency increases by 5% after the sensor is mounted (see Fig. 11).

4. Sensor microfabrication process

The sensor is fabricated on the $\langle 1\,1\,1\rangle$ single crystal silicon by the SCREAM process [17] (or SBM process [18], especially when the silicon substrate is $\langle 1\,1\,1\rangle$, which enables better dimension control giving flat structures after anisotropic etching) as shown in Fig. 12. The thickness of the silicon substrate is 100 μm, which is one-third of the picoslider thickness. The first step of microfabrication is to define piezoresistors using ion implantation. Using diborane ion source, boron ions as the impurity particles were injected into the N-type substrate. The implantation energy used is less than 100 keV to maintain the projected range within 0.5 μm, since the maximum strain is acquired at the top surface of the beam when the beam is deflected. First, low pressure chemical vapor deposition (LPCVD) oxide is deposited on the surface, where mechanical structures are defined. Then deep reactive ion etching is performed and decides the thickness of beams and center plate. Second, LPCVD oxide is covered uniformly on top of etched structures to protect sidewalls from the later wet etching. After
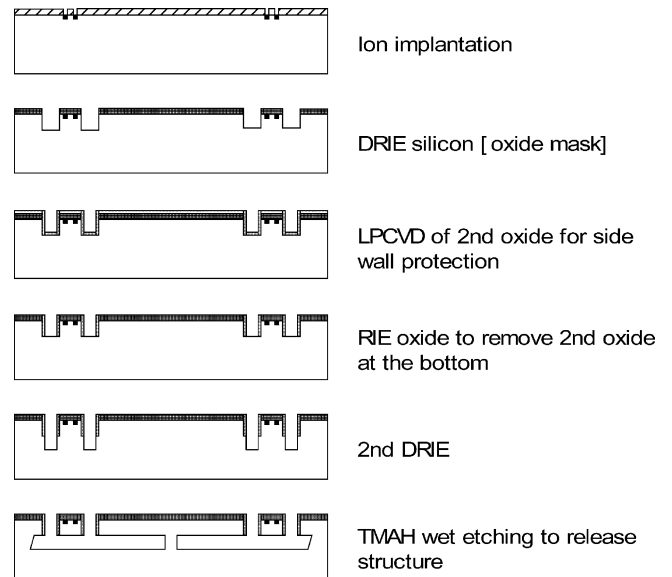

Fig. 12. Fabrication process.

the oxide at the bottom of the trenches are anisotropically removed by reactive ion etching, second DRIE is done determining the supporting column height and the gap between the substrate and beams. As a final step, anisotropic wet etching in TMAH releases the beams and center plates. Using $\langle 1\,1\,1\rangle$ silicon wafer enables flat and uniform beams and center plate after wet etching. The etching time is precisely monitored to control the dimension of supporting column.

Fig. 13 shows the SEM picture of the microfabricated sensor and microscopic photo of the supporting column. The oxide to protect sidewall of the sensor was removed on purpose to monitor the etching time and control the size of the supporting column which cannot be seen otherwise since it is under the silicon center plate. Due to the property of the crystalline structure of $\langle 1\,1\,1\rangle$ single crystal silicon, the column shape is hexagonal as shown in Fig. 13(b) and the major diagonal is still maintained to be less than 9 μm. The
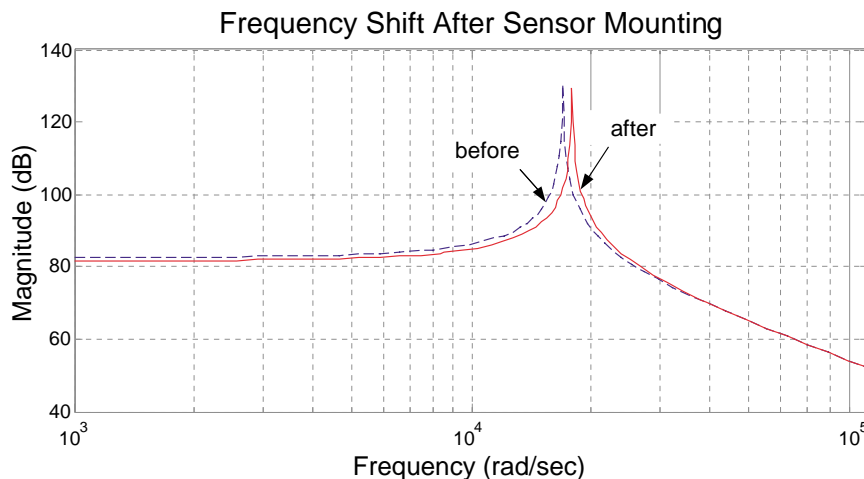

Fig. 11. Comparison of frequency response before/after the sensor mount for the unloaded slider/gimbal system.
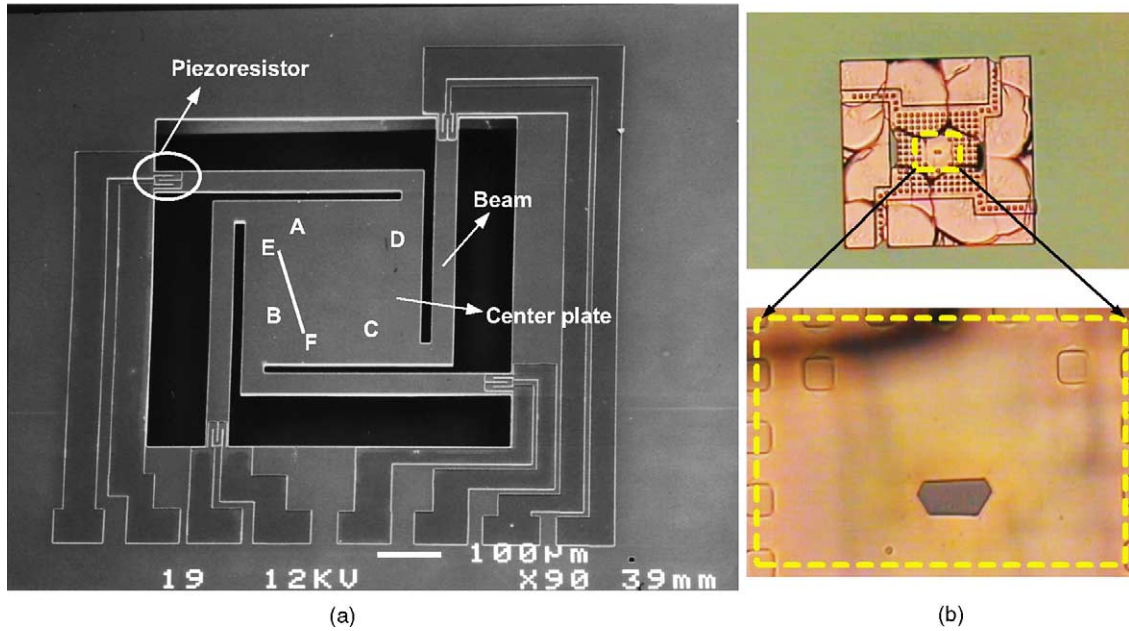
Fig. 13. (a) SEM microphoto of sensor structure and (b) microscopic photo of the supporting column.

precise control of the dimension of this column structure is not easy since it is located under the center plate and requires timed etch. To eliminate this difficulty, test devices were made on another ⟨1 1 1⟩ wafer. In these test devices, the second LPCVD oxide layer to protect side walls described in Fig. 12 is omitted. When the real device wafer is put into the wet etch bath, the test devices are also put in the same bath. By monitoring the etch process through the first transparent oxide layer on the test devices, the etching front can be observed without using the infra-red microscope. We designed several different beam dimensions to characterize the sensitivity of piezoresistors and Fig. 13(b) is the picture of one of the test devices. Since the center plate dimensions are same, the supporting column size in Fig. 13(a) should be close to Fig. 13(b).

5. Sensor calibration and test

The piezoresistors on each beam should be calibrated before it measures pitch and roll angles. Fig. 14 provides the calibration data for one of the beams. The resistance of piezoresistors are in the order of ∼6 kΩ, and the sensitivity defined as resistance change over the unit deflection of the beam is 24 Ω/μm. The gage factor is another important parameter for the sensitivity analysis, which is defined as

$$F = \frac{\mathrm{d}R/R}{\mathrm{d}l/l} = 1 + 2\nu + \frac{\mathrm{d}\rho/\rho}{\mathrm{d}l/l} \tag{3}$$

where l is the length of beam, ν the Poisson's ratio, and ρ is the resistivity of the piezoresistor. The calculated gage factor based on the measurements of the piezoresistor on a beam is 54. Considering the gage factor of metal foil type strain gage is ∼2, our sensor provides much higher sensitivity

and is appropriate for the small motion detection of the gimbal/slider system. As shown in the calibration data, the sensor is also linear for a wide range, which enables the measurement of the relatively big motion of slider in case there are bumps or particles on the rotating disk surface.

To test the performance of the calibrated sensor, the pitch and roll angles measured by the sensor are compared to the optically measured values using white light interferometer. Fig. 15 shows the measured data in two different ways. Each of the four corners, A, B, C, D of the center plate in Fig. 13(a) was poked in turn by a probe and the tilted angle of the center plate with respect to the substrate was first measured using white light interferometer. Then for the same poked position and angle, the output of the piezoresistors on each beam was measured and the pitch and roll angle values were reconstructed using the transformation matrix in Eq. (1). This experiment simulates the pitch and roll motion of the slider when the slider suffers both motion simultaneously.
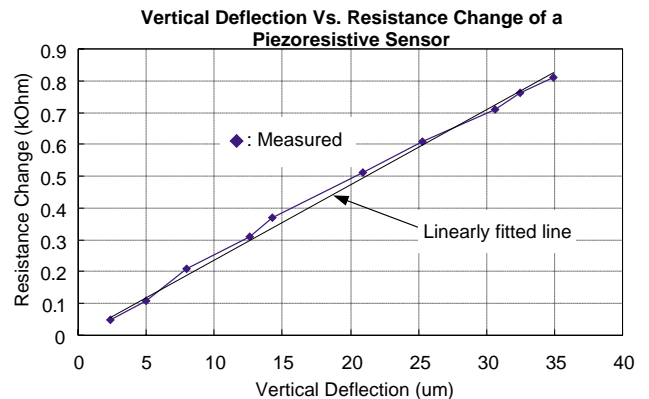

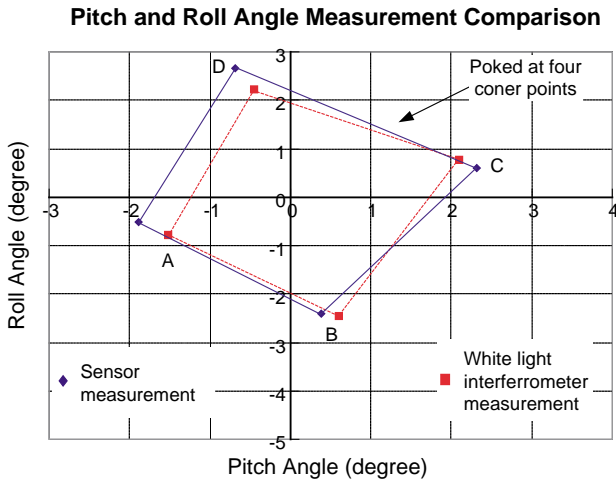Fig. 14. Calibration of the piezoresistor of the sensor.

Pitch and Roll Angle Measurement Comparison

Fig. 15. Performance measurement by poking four corners (WYKO NT3300 was used for comparison).
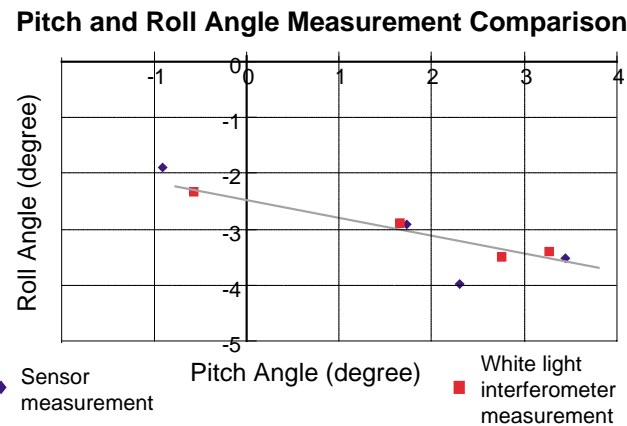
Pitch and Roll Angle Measurement Comparison

Fig. 16. Performance measurement by poking along a line (WYKO NT3300 was used for comparison).

Another measurement result is presented in Fig. 16, where the probe-poking positions follow the line EF in Fig. 13(a) and both pitch and roll angles were measured by the interferometer and the sensor. Both sets of data in Figs. 15 and 16 shows that the pitch and roll angles measured by the sensor follow the interferometric measurement with an average of 14% measurement error that is defined as the summation of percentage errors of each measurement divided by the total number of measurements. Percentage error is calculated as the distance between the sensor and interferometric measurements divided by the distance between the interferometric measurement point and the origin in Figs. 15 and 16.

6. Conclusion

A novel micro sensor was designed and fabricated using the MEMS fabrication technology to detect pitch and roll motions simultaneously in a hard disk slider/gimbal system. The measurement principle and fabrication process were dis-

cussed. The sensor was calibrated and the performance was compared with optical measurement data, which showed good agreement. This sensor has several major merits compared to the existing methods to detect pitch and roll motion of a disk drive system:

1. The sensor would be mounted on a real disk drive system. This enables the test of slider dynamics without using conductive sliders or transparent disks and therefore the measurement data of real magnetic disk and slider could be more accurate.
2. Because the size of the sensor is 25% of the slider size, the undesirable alteration of the system geometry and dynamics is minimized preserving the tribological characteristics of the measured system.
3. The piezoresistor is known to follow high frequency dynamics, which enables in situ measurement of the slider dynamics.

It is expected that this sensor will be useful for the monitoring the slider dynamics and combining this sensor with microactuators designed for high-density data storage devices [19–21] will form a complete feedback loop to improve the performance of hard disk drives. Moreover, MEMS sensor developed in this work could be used as the motion sensor in systems other than the hard disk industry.

Appendix A. Kinematic relation between the beam deflection and the pitch and roll angle

When the slider suffers pitch motion, i.e. Cartesian coordinate system rotates for the pitch angle θ with respect to x-axis in Fig. 5, the new coordinate system (x_i', y_i', z_i') fixed on the slider surface (hence on the outer substrate of the sensor) and the coordinates (x_i, y_i, z_i) fixed on the dimple have the relation

$$\begin{Bmatrix} x_i' \\ y_i' \\ z_i' \end{Bmatrix} = \begin{bmatrix} \cos\theta & 0 & \sin\theta \\ 0 & 1 & 0 \\ -\sin\theta & 0 & \cos\theta \end{bmatrix} \begin{Bmatrix} x_i \\ y_i \\ z_i \end{Bmatrix} \Rightarrow \boldsymbol{X}' = \boldsymbol{PX} \qquad (A.1)$$

and the rotation for the roll angle β with respect to the y-axis gives

$$\begin{Bmatrix} x_i'' \\ y_i'' \\ z_i'' \end{Bmatrix} = \begin{bmatrix} 1 & 0 & 0 \\ 0 & \cos\beta & -\sin\beta \\ 0 & \sin\beta & \cos\beta \end{bmatrix} \begin{Bmatrix} x_i' \\ y_i' \\ z_i' \end{Bmatrix} \Rightarrow \boldsymbol{X}'' = \boldsymbol{RX}'' \qquad (A.2)$$

where (x_i'', y_i'', z_i'') is the coordinates on the slider after pitch and roll motion. Eventually, the coordinates relation between original and new coordinates is

$$
\begin{Bmatrix} x_i'' \\ y_i'' \\ z_i'' \end{Bmatrix} = \begin{bmatrix} \cos\theta & 0 & \sin\theta \\ \sin\beta\sin\theta & \cos\beta & -\sin\beta\cos\theta \\ -\cos\beta\sin\theta & \sin\beta & \cos\beta\cos\theta \end{bmatrix} \begin{Bmatrix} x_i \\ y_i \\ z_i \end{Bmatrix}
$$

$$
\Rightarrow X'' = QX \qquad (A.3)
$$

where $Q = RP$. In general, $RP \neq PR$. However, the angle θ and β are usually small in the slider motion and therefore the transformation matrix can be linearized by setting $\cos\theta \approx 1 \approx \cos\beta$, $\sin\theta \approx \theta$, $\sin\beta \approx \beta$ and $\theta\beta \approx 0$. Then

$$
RP = PR = Q = \begin{bmatrix} 1 & 0 & \theta \\ 0 & 1 & -\beta \\ -\theta & \beta & 1 \end{bmatrix} \qquad (A.4)
$$

Here Q is an orthogonal matrix for the small angle θ and β. The linear translation of the center of the center plate, z_c contributes to each of four beam deflection, z_i and this can be expressed as

$$
\begin{Bmatrix} x_i^* \\ y_i^* \\ z_i^* \end{Bmatrix} = \begin{Bmatrix} x_i'' \\ y_i'' \\ z_i'' \end{Bmatrix} + \begin{Bmatrix} 0 \\ 0 \\ z_c \end{Bmatrix}
$$

$$
= \begin{bmatrix} 1 & 0 & \theta \\ 0 & 1 & -\beta \\ -\theta & \beta & 1 \end{bmatrix} \begin{Bmatrix} x_i \\ y_i \\ z_i \end{Bmatrix} + \begin{Bmatrix} 0 \\ 0 \\ z_c \end{Bmatrix} \qquad (A.5)
$$

Here, we are interested in the total beam deflection, $\Delta z_i = z_i^* - z_i$. By noticing that $x_1 = -a'$, $y_1 = -b'$, $x_2 = -a'$, $y_2 = b$, $x_3 = a$, $y_3 = b$, and $x_4 = a$, $y_4 = -b'$ in Fig. 5 and the transformation relation

$$
z_i^* = -\theta x_i + \beta y_i + z_i + z_c, \quad \Delta z_i = z_i^* - z_i, \qquad (A.6)
$$

the relation between Δz_i and θ, β, z_c can be derived as

$$
\begin{Bmatrix} \Delta z_1 \\ \Delta z_2 \\ \Delta z_3 \\ \Delta z_4 \end{Bmatrix} = \begin{bmatrix} a' & -b' & 1 \\ a' & b & 1 \\ -a & b & 1 \\ -a & -b' & 1 \end{bmatrix} \begin{Bmatrix} \theta \\ \beta \\ z_c \end{Bmatrix} \Rightarrow z_i = T z_c \qquad (A.7)
$$

References

[1] T. Tang, Dynamics of air-lubricated slider bearings for noncontact magnetic recording, Trans. ASME Series F, J. Lubr. Technol. 93 (2) (1971) 272–278.

[2] K. Ono, Dynamic characteristics of air-lubricated slider bearing for noncontact magnetic recording, Trans. ASME Series F, J. Lubr. Technol. 97 (2) (1975) 250–260.

[3] Ta-C. Fu, D.B. Bogy, Slider vibrations induced by ramp-suspension interaction during the ramp loading process, IEEE Trans. Magn. (USA) 30 (6) (1994) 4170–4172.

[4] Q.H. Zeng, D.B. Bogy, A simplified 4-DOF suspension model for dynamic load/unload simulation and its application, Transactions of the ASME, J. Tribol. ASME. 122 (1) (2000) 274–279.

[5] K. Iida, K. Ono, Analysis of bouncing vibrations of a 2-DOF model of tripad contact slider over a random wavy disk surface, Transactions of the ASME, J. Tribol. ASME. 123 (1) (2001) 159–167.

[6] R.F. Hoyt, S.E. Millman, D.E. Horne, Motion pictures of air bearing dynamics under stressed conditions, IEEE Trans. Mag. 23 (5) (1987) 3459–3461.

[7] R. Sonnenfeld, Fly-height, pitch, and crown measurements of hard-disk sliders by capacitance stripe, IEEE Trans. Mag. 28 (5) (1992) 2545–2547.

[8] R. Sonnenfeld, Capacitance methods in head-disk interface studies, IEEE Trans. Mag. 29 (1) (1993) 247–252.

[9] G.L. Best, Comparison of optical and capacitive measurements of slider dynamics, IEEE Trans. Mag. 23 (5) (1987) 3453–3455.

[10] X. Liu, W. Clegg, B. Liu, Normal incidence polarization interferometer for measuring flying height of magnetic heads, IEEE Trans. Mag. 35 (5) (1999) 2457–2459.

[11] J.F. Burger, G.-J. Burger, T.S.J. Lammerink, S. Imai, J.H.J. Fluitman, Miniaturised friction force measuring system for tribological research on magnetic storage devices, in: Proceedings of the IEEE, The Ninth Annual International Workshop on Micro Electro Mechanical Systems, New York, NY, USA, 1996, pp. 99–104.

[12] Y. Hu, P.M. Jones, K. Li, Air bearing dynamics of sub-ambient pressure sliders during dynamic unload, ASME/STLE, in: Proceedings of the International Tribology Conference, Toronto, Canada, 25–28 October 1998.

[13] J.P. Peng, Theoretical prediction of ramp loading/unloading process in hard disk drives, ASME/STLE, in: Proceedings of the International Tribology Conference, Toronto, Canada, 25–28 October 1998.

[14] Q.H. Zeng, M. Chapin, D.B. Bogy, Dynamics of the unload process for negative pressure sliders, IEEE Trans. Mag. 35 (2) (1999) 916–920.

[15] Q.H. Zeng, D.B. Bogy, Slider air bearing designs for load/unload applications, IEEE Trans. Mag. 35 (2) (1999) 746–751.

[16] L. Muller, Gimballed Electrostatic Microactuators with Embedded Interconnects, PhD Thesis, University of California, 2000.

[17] K.A. Shaw, Z.L. Zhang, N.C. MacDonald, SCREAM I: a single mask, single-crystal silicon, reactive ion etching process for microelectromechanical structures, Sens. Actuators A, Phys. A40 (1) (1994) 63–70.

[18] L. Sangwoo, P. Sangjun, D.-I. Cho, The surface/bulk micromachining (SBM) process: a new method for fabricating released MEMS in single crystal silicon, J. Microelectromech. Syst. 8 (4) (1999) 409–416.

[19] D.A. Horsley, R. Horowitz, A.P. Pisano, Microfabricated electrostatic actuators for hard disk drives, IEEE/ASME Trans. Mechatronics 3 (3) (1998) 175–183.

[20] L. Muller, A.P. Pisano, R.T. Howe, Microgimbal torsion beam design using open, thin-walled cross sections, J. Microelectromech. Syst. 10 (4) (2001) 550–560.

[21] W. Tang, V. Temesvary, J.J. Yao, Y.-C. Tai, D.K. Miu, Silicon microactuators for computer disk drives, Jpn J. Appl. Phys., Part 1 35 (1B) (1996) 350–356.

Biographies

Jongbaeg Kim received the BS degree in mechanical engineering from Yonsei University, Korea in 1997 and the MS degree in mechanical engineering from the University of Texas at Austin, TX in 1999. He is currently working toward the PhD degree in mechanical engineering at the University of California at Berkeley as a researcher at Berkeley Sensor and Actuator Center. His research interests are system dynamics, modeling, design, and fabrication of MEMS and nanotechnology.

Liwei Lin received the MS and PhD degrees in mechanical engineering from the University of California, Berkeley, in 1991 and 1993, respectively. He joined BEI Electronics Inc. USA from 1993 to 1994 in microsensors research and development. From 1994 to 1999, he was an associate professor in the Institute of Applied Mechanics, National Taiwan University, Taiwan and later an assistant professor at the Mechanical Engineering and Applied Mechanics Department at the University of Michigan. He joined the University of California at Berkeley in 1999 and is now an associate professor at Mechanical Engineering Department and Co-Director at Berkeley Sensor and Actuator Center, NSF/Industry/University Research Cooperative Center. His research interests are in design, modeling, and fabrication of microstructures, microsensors, and microactuators as well as mechanical issues in microelectromechanical systems and he holds eight US patents. Dr. Lin is the recipient of the 1998 NSF CAREER Award for research in MEMS Packaging and the 1999 *ASME Journal of Heat Transfer* best paper award for his work on micro scale bubble formation and is a subject editor for the *IEEE/ASME Journal of Microelectromechanical Systems*. He served as Chairman of the Micromechanical Systems Panel of the ASME Dynamic Systems and Control Division in 1997 and 1998 and led the effort in establishing the MEMS sub-division in ASME and is currently the Vice Chairman of the executive committee.